Opto-Electronics Review

Thermal analysis of a two-dimensional array with surface light emission based on nitride EEL lasers

Dominika Dąbrówka[a]*, Robert P. Sarzała[a], Michał Wasiak[a], Anna Kafar[b], Piotr Perlin[b], Kiran Saba[b]

[a] Institute of Physics, Lodz University of Technology, 217/221 Wólczańska St., 93-005 Łódź, Poland
[b] Institute of High Pressure Physics, Polish Academy of Sciences, 29/37 Sokołowska St., 01-142 Warsaw, Poland

Article info	Abstract
	This paper presents the results of a thermal computational analysis of a two-dimensional laser array emitting from a surface. The array consisted of eight equispaced ridge-waveguide edge-emitting nitride diode lasers. Surface emission of light was obtained using mirrors inclined at 45°. The authors investigate how the geometrical dimensions of the array emitters and their pitch in the array affect the increase and distribution of temperature in the device. They also examine the influence on the temperature increase and distribution of the thickness of the insulating SiO_2, the thickness of the gold layer forming the top contact of the laser, and the thickness of the GaN substrate, as well as the influence of the ridge-waveguide width.

1. Introduction

Semiconductor light sources based on III-N materials enable the emission of radiation in the visible spectrum. Such semiconductors have various applications – e.g., in colour displays, pico projectors, translucent displays, lighting devices, high-resolution printing, wireless optical communication in the visible range, underwater communication, lidars, medical diagnostics, biosensors, and spectrometers. In many of these applications, the power of the emitted light and the shape of the optical beam are important. It is often desirable to emit light from the surface of the device. This allows for easy scaling of optical power. It gives the device better thermal properties and enables better coupling of the emitted beam with other optoelectronic elements. These features can be achieved by building two-dimensional (2D) laser arrays emitting from the surface.

A natural candidate for a single emitter in such an array is a vertical cavity surface emitting laser (VCSEL). The 2D VCSEL arrays produced commercially are based on arsenide material systems and emit powers up to the order of kW [1]. Unfortunately, such arrays emit radiation only in the near infrared spectral range. Nitride VCSELs still have several weaknesses and limitations, despite huge progress in recent years [2]. Nitride VCSELs emitting over

10 mW have been reported [3] which were tested in a 2D array containing 256 individual emitters [4]. However, the array emitted only 1 W of power.

Only edge-emitting lasers (EELs) are commercially available for use as blue light emitters [5]. One-dimensional (1D) matrices of blue EELs can be made, usually, consisting of several devices [6]. An alternative approach is to construct a 2D array based on EELs, in which the emitted beam is directed upwards – e.g., by means of external mirrors directed at an angle of 45°. This idea was presented in 1977 for lasers made in the arsenide technology [7–9]. However, the concept was later abandoned, mainly because VCSEL technology and the technology for 2D VCSEL arrays had been well mastered. In the case of VCSELs built in nitride technology, which still presents a significant challenge, the concept of a 2D EEL array emitting upwards may be a good solution. The high thermal conductivity of GaN could be very beneficial in the case of 2D matrices.

This paper presents the results of a thermal computational analysis of a 2D array of nitride EELs. The examined array consisted of eight emitters. Surface emission of light was obtained using mirrors inclined at an angle of 45° which redirected most of the emitted radiation upwards. The authors investigated the influence of the geometrical dimensions of the array emitters and their alignment in the array on the temperature increase and

distribution in the device. The influence of the thickness of the SiO$_2$ insulating layer, the thickness of the gold layer forming the top contact of the laser, the GaN thickness, and the ridge-waveguide width have also been examined. Particular attention was given to the self-heating effect of the individual emitters of the array. To the best knowledge of the authors, this is the first analysis of a 2D array of nitride EELs. It, therefore, marks the first step towards the design and production of this type of array.

2.   Structure

Simulations were conducted to facilitate further design and technological work. The modelled array consists of nitride EELs. The emitted beam was directed upwards by slanted mirrors (see Fig. 1). Such a geometry of the emitter is possible to be fabricated thanks to patterning the GaN substrate prior to the metalorganic vapour-phase epitaxy (MOVPE) to create the 45° inclined planes. Next, the growth and processing are performed. As one of the final steps of the processing, the vertical etching is made which defines the laser cavity, as well as lowers the 45° mirrors so that the laser beam is incident on the middle of the mirror. The single array emitter was designed to emit a wavelength of around 430 nm. Details of the construction are given in Fig. 1, Fig. 2, and Table 1. Such a single laser was fabricated, and its experimental light-current-voltage (LIV) curve is presented in Fig. 3. Table 1 also includes thermal conductivities of the materials at 300 K which were used in the simulations. Calculations by the transfer-matrix method give the reflectivity of the 45° mirror of around 8.7% which is quite low. That is why it is preferred to coat the mirror with high reflection coatings.
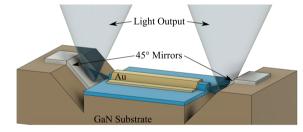

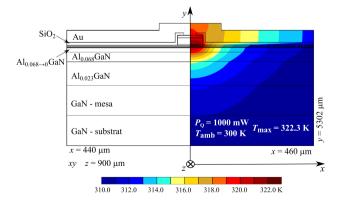**Fig. 1.** Schematic of the laser used to build the simulated array (not to scale).

Fig. 2. Cross-section at the half-length of a single emitter: schematic of the layers (left) and the calculated temperature distribution inside the emitter (right), assuming a dissipated thermal power of 1 W and a heat sink temperature of 300 K (figure to scale).

Table 1.
Details of the layers used in the EEL structures (Fig 2): d denotes the thickness of the layer, thermal conductivities k are at 300 K [10–14].

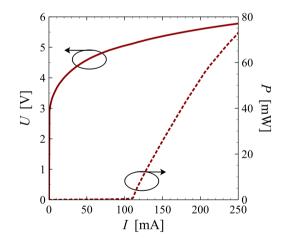| Material		d [nm]	$k \left[\dfrac{\text{W}}{\text{m} \cdot \text{K}}\right]$
u−Au		1000	319.0
u−SiO$_2$		200.0	1.38
p−GaN		210.0	78.80
p−Al$_{0.045}$GaN		550.0	46.49
p−Al$_{0\to0.045}$GaN		100.0	92.52
p−(Al$_{0.12}$GaN/GaN) × 9		2.0/2.0	21.50/43.86
p−Al$_{0.12}$GaN		2.0	21.50
p−GaN		2.0	50.72
p−In$_{0.043}$GaN		65.0	15.10
GaN	QB	4.0	55.04
In$_{0.12}$GaN	QW$_{deep}$	3.1	6.13
In$_{0.06}$GaN	QW$_{shallow}$	1.3	11.21
GaN	QB	5.0	56.51
In$_{0.12}$GaN	QW$_{deep}$	3.1	6.13
In$_{0.06}$GaN	QW$_{shallow}$	1.3	11.21
GaN	QB	5.0	56.51
n−In$_{0.043}$GaN		50.0	15.10
n−GaN		10.0	60.20
n−Al$_{0.068\to0}$GaN		350.0	74.82
n−Al$_{0.068}$GaN		800.0	33.72
n−Al$_{0.023}$GaN		$2.0 \cdot 10^3$	75.07
u−GaN (substrate)		$300.0 \cdot 10^3$	150.0
u−PbSn (solder)		$5.0 \cdot 10^3$	50.0
u−Cu (heat sink)		$5000.0 \cdot 10^3$	400.0

Fig. 3. Measured LIV characteristics of an EEL similar to those used in the array.

The lasers used in the array are ridge lasers (the ridge width was assumed to be 2 µm) with two quantum wells in the active region. The wells are made of InGaN with different indium compositions. They are divided between a deeper part (QWdeep) and a shallower part (QWshallow). The barriers (QBs) separating the wells are made of gallium nitride. The active region is surrounded by p-type and n-type

waveguide and cladding layers. At the very top, there is a gold layer which acts as an electrical contact and a heat spreading layer. Outside the ridge, on almost the entire surface, the gold layer is separated from the structure by a 200 nm thick silicon dioxide insulating layer (see Fig. 2). The laser and the whole array were made on a 300 μm thick gallium nitride substrate with lateral dimensions of 4.5 mm × 4.5 mm, and then attached to a copper heat sink with dimensions of 2 cm × 2 cm and a thickness of 5 mm. The device was mounted on a copper heat sink using tin-lead (PbSn) solder.

3. Numerical model

The simulations were performed using a program written by the Photonics Group of the Institute of Physics at Lodz University of Technology. The program simulates physical phenomena occurring during the operation of semiconductor lasers and their arrays [15]. The part used to model thermal phenomena is based on a 3D finite element method (FEM). In this paper, the continuous wave (CW) operation of the array is analysed. In this case, the equation of thermal conductivity can be written as follows

$$\nabla \cdot [k(x,y,z) \times \nabla(T(x,y,z))] = -g(x,y,z), \qquad (1)$$

where k is the thermal conductivity, T is the temperature, and g is the volumetric power density of heat sources. For the performed calculations, it was assumed that the heat was generated in particular layers of the laser, with the greatest amount of heat (50%) generated in the active area. Distribution of the remaining half of the power is shown in Table 2. This heat sources distribution is taken from self-consistent electrical-thermal simulations of the single emitter. Additionally, calculations for the case where 100% of the power is in the active region of the laser were performed. The difference in temperature increases between these two analysed cases is less than 10% in favour of the distribution presented in Table 2.

Table 2.
Assumed percentage of generated power $D_\%$ in the laser areas and layer thicknesses d.

Layer	d [nm]	Percentage of generated power $D_\%$
p–GaN	210.0	20%
p–Al$_{0.045}$GaN	550.0	20%
p–Al$_{0\rightarrow0.045}$GaN	40.0	2%
p–Al$_{0\rightarrow0.045}$GaN	60.0	3%
p–Al$_{0.12}$GaN/GaN	40.0	2%
p–In$_{0.043}$GaN	65.0	3%
Active region	22.8	50%

The appropriate value of the power density g was obtained by dividing the percentage of power dissipated in the given region by the volume of that region V_a:

$$g = \frac{D_\% \cdot P_Q}{V_a} = \frac{D_\% \cdot P_Q}{d \cdot S_{RW} \cdot L}. \qquad (2)$$

The layers given in Table 2 have their widths equal to the width of the ridge S_{RW}. The thicknesses d is given in Table 2. The length L is equal to the length of the laser (parameter L in Fig. 4).

The authors assume that the side and top walls of the laser are thermally isolated, and the bottom of the copper heat sink is kept at a constant temperature of 300 K.

The calculations were performed in a self-consistent manner, assuming that the thermal conductivity of the semiconductor layers forming the laser varied with temperature. A more detailed description of the model may be found in Refs. 16 and 17. The temperature dependence of the thermal conductivity is expressed by the temperature coefficient δ and is as follows:

$$k(T) = k(300 \text{ K}) \cdot \left[\frac{T}{300 \text{ K}}\right]^\delta. \qquad (3)$$

The temperature coefficient $\delta = -1.4$ was used for the layers forming the QWs, the Al$_{0.045}$GaN and Al$_{0.068}$GaN gradient layers, and the GaN substrate. However, the thermal conductivities of gold, silicon dioxide, copper, and tin-lead solder were assumed to be constant because in the considered temperature range their slight changes do not have any significant impact on the results. The values for thermal conductivity at room temperature used in the simulation are given in Table 1, which also gives detailed information on the structure of a single emitter [10–14].

4. Results

The simulation began by determining the temperature distribution for different powers of the heat sources, in a single emitter located at the centre of the substrate. The dimensions of the substrate (4.5 mm × 4.5 mm × 300 μm) and heat sink (2 cm × 2 cm × 5 mm) were the same as for the array. The maximal temperatures for single emitters are given in Table 3.

Table 3.
Maximum temperature T_{max} in a single emitter array and thermal resistance R_{th} for three values of laser length L and heat source powers in the single emitter of 1, 2, and 3 W.

Power in the single emitter	1 W		2 W		3 W	
L [μm]	T_{max} [K]	R_{th} [K·W⁻¹]	T_{max} [K]	R_{th} [K·W⁻¹]	T_{max} [K]	R_{th} [K·W⁻¹]
600	334.3	34.3	373.1	36.6	417.0	39.0
900	322.3	22.3	346.5	23.3	372.7	24.2
1200	316.9	16.9	335.0	17.5	354.3	18.1

The temperature distributions were obtained for three different values of the laser length L. For each of the three values of L, the temperature distributions were also obtained for three different powers of the heat source. The highest temperatures in the array are shown in Table 3. The temperature rise above the temperature of the heat sink (ΔT) in the reference array ($L = 900$ μm) was 22.3 K for 1 W of heat power (see Fig. 2). As can be seen in Table 3,

for each considered value of the parameter L, a two-fold increase in the heat source power (from 1 W to 2 W) only slightly exceeds more than doubling of ΔT. The observed temperature changes are nonlinear with the increase of the separated power in the emitter. The temperature isotherms inside the 900 µm laser are shown on the right side in Fig. 2. As can be seen, the temperature rise occurs mainly in the immediate surroundings of the active region, in the ridge-waveguide, and in the gold contact located directly above the waveguide.

Subsequently, calculations were performed for laser arrays with eight lasers. The number of emitters per surface unit is a key parameter for a laser matrix. For this reason, the authors analysed three values of parameter A (see Fig. 4) which determines the length of a single laser ridge, the distance between the facets of adjacent emitters (along the z axis), and the pitch along the x axis. As a result, there are 16 evenly distributed points emitting light on the surface of the array.

Knowing the maximum values and temperature distributions in a single emitter, a thermal analysis of eight-element arrays was performed. As already mentioned, the emitters in the array are arranged to form 16 evenly spaced light sources on the surface (see the red dots in Fig. 4). An array with $A = 900$ µm was used as the reference array. A comparison of the results in Table 3 (for $L = 900$ µm) and Table 4 shows that in the reference structure the thermal interaction between the emitters is not particularly strong. This is confirmed by the isotherms shown in Fig. 4 which were drawn for the active-region plane and are very similar for all the emitters. The lack of interaction is due to the large distances between the ends of the waveguides, vertically and horizontally (parameter A).

Table 4.
Maximum temperatures and thermal resistance R_{th} in four emitters closest to the centre of the array (L11) and four outermost emitters (L12) (see Fig. 4) obtained for three different heat source powers in each emitter located in the array and $A = L = 900$ µm.

Power per emitter in the array	L11 emitter		L12 emitter	
	T_{max} [K]	R_{th} [K·W⁻¹]	T_{max} [K]	R_{th} [K·W⁻¹]
1 W	324.1	24.1	323.7	23.7
2 W	350.4	25.2	349.5	24.8
3 W	379.2	26.4	377.6	25.9

Figure 5(a) shows the dependence of the maximum temperature in the array on parameter A, obtained for heat sources of 1, 2, and 3 W. For the lowest considered power when A is reduced from 900 µm to 600 µm, the temperature increases by around 56%. When A is changed from 900 µm to 1200 µm, the temperature falls by around 24%. Reducing the length of the emitters and bringing them closer together causes a significant increase in temperature in the upper structural elements [see Fig. 5(b)]. This increase is mainly caused by the varying density of the heat source. The thermal crosstalk remains small, even for the smallest distances considered [see Fig. 5(c)]. In the case of higher powers, greater relative temperature variations are observed (between a 65% increase and a 26% decrease for 3 W per emitter).

Next, the influence of the thickness of the upper gold contact was examined. The gold contact is the uppermost layer in the emitter. Its main function is to act as a positive
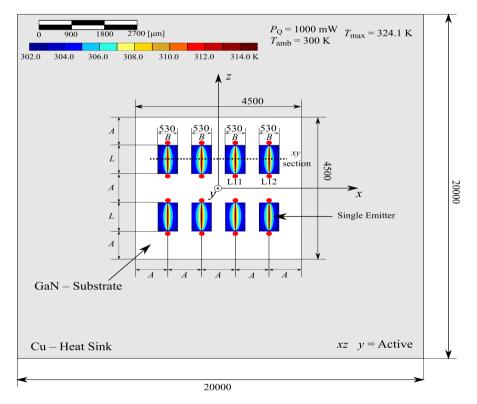

Fig. 4. Top view of the eight-element EEL array with the most important dimensions marked. The temperature distribution in the xz section at the active region obtained for the reference structure ($A = L = 900$ µm) is also shown. All dimensions are given in µm. The emitted light sources are marked with red points in the diagrams.
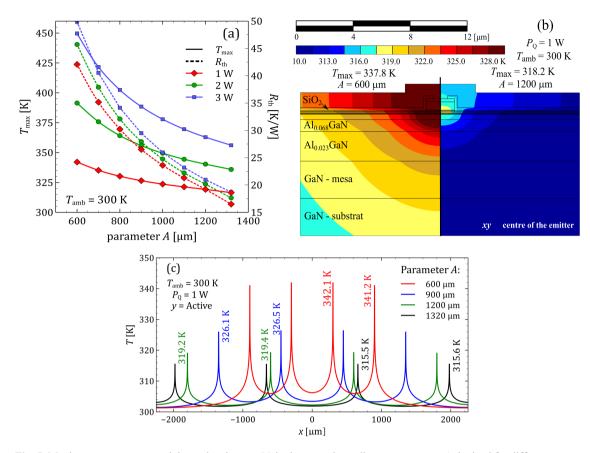
Fig. 5. Maximum temperature and thermal resistance (a) in the array depending on parameter A obtained for different powers of heat sources in the emitter; temperature distributions (b) around the active region of the emitter L11 [in the centre of the emitter, xy section (see Fig. 4)] in an 8-element EEL laser array where $A = 600$ µm (on the left) and $A = 1200$ µm (on the right), and the heat source power for a single emitter is 1 W. Temperature distributions (c) at the x-coordinate, at the height y corresponding to the centre of the active region, and the z-coordinate corresponding to the centre of the emitter [xy section (see Fig. 4)].

electrode. It also acts as a heat spreader, allowing for a more efficient heat transport from the active region to the heat sink and reducing temperature in the entire structure. In the reference structure, the thickness of the gold layer is 1 µm. Figure 6(a) shows the impact of the thickness of the gold layer (d_{Au}) on the maximum temperature T_{max} in the case of a heat source power of 1 W.

As can be seen, significant changes in the maximum temperatures and their distributions occur when d_{Au} is varied. A gold layer thinner than 1 µm results in a significant increase in temperature of the active regions of the emitters. When d_{Au} is reduced from 1 µm to 0.4 µm, temperature increases by about 12%. As can be seen from Fig. 6, a further improvement in the thermal properties of
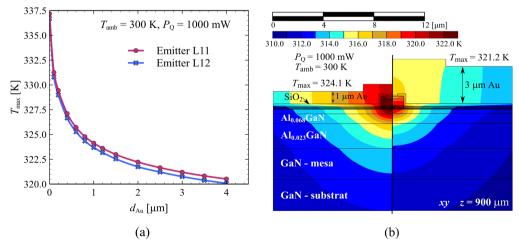

Fig. 6. Maximum temperature (a) in array emitters depending on the thickness of the gold layer for the inner emitters (L11) and outermost emitter (L12); temperature distributions (b) in L11 obtained for the reference thickness of the gold layer: $d_{Au} = 1$ µm (on the left) and for the increased thickness $d_{Au} = 3$ µm (on the right). The cross-section plane refers to the centre of the emitter.

the array may be achieved by increasing the thickness of the gold up to 2 μm or 3 μm. A 3 μm thick layer reduces the temperature increase by about 12% relative to a 1 μm layer. Complete elimination of the gold layer causes a temperature increase of 54%.

The influence of adding another layer in the emitter was also analysed. This SiO_2 layer isolated the gold electrode from the semiconductor structure in the area of the ridge side walls and outside the ridge, leaving only a 1 μm wide electric contact at the top of the ridge. This defined the width of the current injection region. The thickness of the SiO_2 layer should not be too low, due to the risk of electrical breakdown when the laser is biased. The calculations showed that even doubling the thickness of the SiO_2 layer from 200 nm to 400 nm results in a temperature increase of less than 2%. This means that the thickness of the layer can be safely increased to a certain extent, although a perfectly thermally insulating SiO_2 layer would increase the temperature rise by a significant 46%.

The analysed array is assumed to be grown on a gallium nitride substrate. The substrate is one of the most important elements of the array, from the point of view of the thermal properties of the device. Thanks to its high thermal conductivity, it acts as an effective heat spreader, provided that its thickness is properly chosen. Another important parameter is the quality of the thermal contact between the substrate and the heat sink. In the authors' simulations, the quality of the thermal contact is expressed by the value of the effective thermal conductivity of the PbSn solder (α_{PbSn}) [18, 19]. Three realistic values were considered: 10, 20, and 40 W/cm²·K. However, in the case of a perfect thermal connection between the solder, the heatsink, and the substrate, the effective thermal conductivity is 1000 W/cm²·K.

The results of the simulations are shown in Fig. 7. The calculations were performed using the most commonly assumed value for the thermal conductivity of GaN substrates, 150 W/m·K [20]. Calculations for 50 W/m·K which is close to the thermal conductivity of gallium arsenide were also performed [21]. This enabled a comparison of the thermal properties of the analysed nitride array with a similar array made in arsenide technology.

The results show that a reasonable thickness for a GaN substrate is between 100 and 200 μm. For a power of 1 W per emitter and in the case of a heat transfer coefficient of the solder in the range of 10–40 W/cm²·K, the maximum temperature increase in the array is 25–30 K. A further increase in the substrate thickness does not significantly reduce the temperature in the array. Differences in the temperature rise when the GaN substrate has a thickness of 200 μm and when it has a thickness of 300 μm are at most 0.5 K. As can be seen in Fig. 7, reducing the thickness below 100 μm causes a rapid deterioration of the thermal conditions inside the device.

Figure 7 also shows that an analogous array made on a GaAs substrate would have significantly worse thermal properties than an array made on a GaN substrate. The increase of the temperature in the emitters of a device on a GaAs substrate would be 40–70% greater.

The emitters in the array are assumed to be ridge-waveguide EELs. The width of a ridge in a nitride EEL is usually from 1 to several μm. In this paper, the authors studied the effect of varying the ridge width between
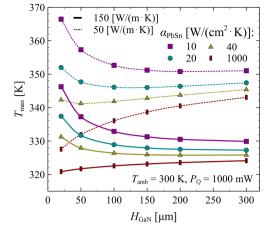

Fig.7. Maximum temperature depending on the layer thickness H_{GaN}, thermal conductivity k_{GaN} of the GaN substrate, and different values of the heat transfer coefficient of the solder α_{PbSn}.

2–15 μm on the thermal properties of the array. The calculations assume that the width of the electric contact is 1 μm smaller than the ridge width and that the power of the heat source is kept constant. The results are shown in Fig. 8 for the highest considered value of the thermal conductivity of the solder and for five different values of the heat source power. The reduction in temperature caused by widening of the ridge is a result of lowering the density of the heat sources power. However, this reduction is not proportional to the increase in the volume of the active region. The temperature rise for an array with emitters with a ridge width of 15 μm is almost 30% smaller than in the case of an array made of lasers with a ridge width of 2 μm, while the density of the heat sources fell 8-fold.
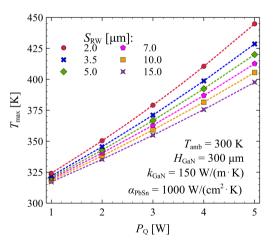

Fig. 8. Dependence of the maximum temperature in the array on the power of the heat source P_Q dissipated in each of the emitters, for different widths of the emitter ridge-waveguide S_{RW}.

5.   Conclusions

This paper has presented a theoretical thermal analysis of a 2D surface emission array consisting of eight edge emitting lasers to which 45° mirrors are attached enabling light emission from the surface. In an array where the distance between the emitters is equal to 900 μm, there is no strong thermal interaction between the emitters. The

increase in the maximum temperature in the array is about 8% higher than for a single laser array placed on the substrate and heat sink. Reducing the distance between the emitters leads to a more pronounced crosstalk. For example, for a distance between emitters equal to 600 μm, a temperature increase of 56% can be observed.

The maximum temperature increase in the array was found to depend strongly on the thickness of gold placed on the top surface of a single emitter. With a gold layer thickness of 4 μm, the temperature increase was 40% lower than for an emitter with no gold layer. The thickness of a SiO_2 layer insulating the top electrode from the semiconductor was found to have no significant influence on the temperature increase in the array. From the point of view of the laser thermal properties, the optimal thickness of the GaN substrate was determined to be in the range of 100–200 μm. However, this value depends on the quality of the solder and the quality of GaN itself.

A comparison between the GaN substrate with a hypothetical GaAs substrate revealed a 40–70% higher temperature increase in the array based on GaN.

Acknowledgements

References

[1] Warren, M. E. *et al*. High-speed and scalable high-power VCSEL arrays and their applications. *Proc. SPIE* **9381**, (2015). https://doi.org/10.1117/12.2080235

[2] Huang, C. Y. Challenges and advancement of blue III-Nitride vertical-cavity surface-emitting lasers. *Micromachines* **12**, 676 (2021). https://doi.org/10.3390/mi12060676

[3] Kuramoto, M. *et al*. High-power GaN-based vertical-cavity surface-emitting lasers with AlInN/GaN distributed Bragg reflectors. *Appl. Sci.* **9**, 416 (2019). https://doi.org/10.3390/app9030416

[4] Kuramoto, M. *et al*.Watt-class blue vertical-cavity surface-emitting laser arrays. *Appl. Phys. Express* **12**, 091004 (2019). https://doi.org/10.7567/1882-0786/ab3aa6

[5] Liu, J. *et al*. GaN-based blue laser diodes with 2.2 W of light output power under continuous-wave operation. *IEEE Photon. Technol. Lett.* **29**, 2203–2206 (2017). https://doi.org/10.1109/LPT.2017.2770169

[6] Perlin, P. *et al*. InGaN laser diode mini-arrays. *Appl. Phys. Express* **4**, 062103 (2011). https://doi.org/10.1143/apex.4.062103

[7] Springthorpe, A. J. A novel double-heterostructure p-n junction laser. *Appl. Phys. Lett.* **31**, 524 (1977). https://doi.org/10.1063/1.89762

[8] Donnelly, J. P., Rauschenbach, K., Wang, C. A., Goodhue, W. D. & Bailey, R. J. Two-dimensional surface-emitting arrays of GaAs/AlgaAs diode lasers. *Proc. SPIE* **1043**, *Laser Diode Technology and Applications* (1989). https://doi.org/10.1117/12.976359

[9] Kim, J. H., Lang, R. J. & Larsson A. High-power AlGaAs/GaAs single quantum well surface-emitting lasers with integrated 45° beam deflectors. *Appl. Phys. Lett.* **57**, 2048–2050 (1990). https://doi.org/10.1063/1.103937

[10] Śpiewak, P. *et al*. Impact of thermal crosstalk between emitters on power roll-over in nitride-based blue-violet laser bars. *Semicond. Sci. Technol.* **32**, 025008 (2017). https://doi.org/10.1088/1361-6641/aa513b

[11] Shackelford, J. F. & Alexander, W. *CRC Materials Science and Engineering Handbook*, *Third Edition*. (CRC Press, 2001). https://doi.org/10.1201/9781420038408

[12] Lide, D. R. CRC handbook of chemistry and physics: a ready-reference of chemical and physical data, 85th edition. *J. Am. Chem. Soc.* **127**, 4542 (2004). https://doi.org/10.1021/ja041017a

[13] Kuc, M. & Sarzała, R. P. *Modelowanie zjawisk fizycznych w krawędziowych laserach azotkowych oraz ich matrycach*. (Wydawnictwo Politechniki Łódzkiej, 2016). [in Polish]

[14] Nakwaski, W. Thermal conductivity of binary, ternary, and quaternary III–V compounds. *J. Appl/ Phys.* **64**, 159–166 (1988). https://doi.org/10.1063/1.341449

[15] Sarzała, R. P., Śpiewak, P., Nakwaski, W. & Wasiak, M. Cavity designs for nitride VCSELs with dielectric DBRs operating efficiently at different temperatures. *Opt. Laser Technol.* **132**, 106482 (2020). https://doi.org/10.1016/j.optlastec.2020.106482

[16] Karbownik, P. & Sarzała, R. Structure optimisation of short-wavelength ridge-waveguide InGaN/GaN diode lasers. *Opto-Electron. Rev.* **16**, 27–33 (2008). https://doi.org/10.2478/s11772-007-0035-3

[17] Tomczyk, A., Sarzała, R. P., Czyszanowski, T., Wasiak, M. & Nakwaski, W. Fully self-consistent three-dimensional model of edge-emitting nitride diode lasers. *Opto-Electron. Rev.* **11**, 65–75 (2003). https://www.infona.pl/resource/bwmeta1.element.baztech-article-BWA1-0002-0110

[18] Chung, D. D. L. Thermal interface materials. *J. Mater. Eng. Perform.* **10**, 56–59 (2001). https://doi.org/10.1361/105994901770345358

[19] Khounsary, A. M., Chojnowski, D., Assoufid, L. & Worek, W. M. Thermal contact resistance across a copper-silicon interface. *Proc. SPIE* **3151**, 45–51 (1997). https://doi.org/10.1117/12.294497

[20] Wengang, W. B., Haochung, H. K., Peicheng, K. & Shen, B. *Handbook of GaN Semiconductor. 1st edition* (CRC Press, 2017). https://doi.org/10.1201/9781315152011

[21] Adachi, A. *Properties of Semiconductor Alloys: Group-IV, III–V and II–VI Semiconductors*. (John Wiley & Sons, Ltd., 2009). https://doi.org/10.1002/9780470744383